Functional Neuroimaging

TECHNICAL FOUNDATIONS

Edited by

Robert W. Thatcher
M. Hallett
T. Zeffiro
E. Roy John
Michael Huerta*

Medical Neurology Branch
Clinical Neuroscience Division
National Institute of Neurological Disorders & Stroke
National Institutes of Health
Bethesda, Maryland

** Division of Neuroscience & Behavioral Science*
National Institute of Mental Health
National Institutes of Health
Rockville, Maryland

Academic Press
San Diego New York Boston London Sydney Tokyo Toronto

8

Statistical Parametric Mapping

Karl J. Friston

The Neurosciences Institute, La Jolla, California 92037

I. Introduction

This chapter describes the ideas and techniques used in statistical parametric mapping. In one sense, statistics are the ultimate modality. They are dimensionless and allow information from different modalities to be compared or correlated. Statistical parametric maps (SPMs) are images with pixel values that are, under a null hypotheses, distributed according to a known (statistical) probability density function. SPMs are used to test specific null hypotheses, usually an equivalence or regional physiology or absence of correlation. SPMs are essentially images of change or correlational significance. Statistical parametric mapping involves a variety of analytical techniques. Those described here represent an internally consistent series of data transformations developed at the MRC Cyclotron Unit (Hammersmith Hospital, London). Each transformation appeals to a distinct and separate theory. The endpoint of these data transformations is the SPM.

Pixel values in the SPM are a statistical quotient, usually of the variance (differences) of interest and error variance (reliability) of the measurement. Increasing sensitivity means reducing of error variance. The remodeling and reduction of error variance is a constant theme found throughout the data analysis stream. The efficacy and nature of each data transformation are defined in terms of the error variance it addresses. This is reflected in the descriptions below, which are structured around the source of error reduced and are presented in the order in which the transformations are performed. The most common experimental design, of repeated observations in different subjects, is the sensorimotor or cognitive activation paradigm. Consequently the analysis of activation studies will form the core of this chapter, namely the general case of k repeated measurements in n subjects.

The first half describes how SPMs are constructed. The second half provides empirical examples that show how SPMs can be used to assess (i) functional anatomy and specialization using activation studies, (ii) CNS plasticity with factorial designs, and (iii) functional connectivity using principal component analyses. The first half is a little dense and some readers may prefer to go straight to the second half and refer back for technical details.

II. Procedures

A. The Physiological Measurement

Neurophysiology is usually measured in terms of regional cerebral blood flow (rCBF), typically with a fast dynamic technique using ^{15}O radiolabeled water, administered intravenously or by $C^{15}O_2$ inhalation. Counts per pixel, per unit time, integrated over the

acquisition period can be used as an index of rCBF or entered into a more complete analysis to generate images of actual rCBF using parameter estimation (Lammertsma *et al.*, 1990). This parameterization removes variability due to technical idiosyncrasies but preserves rCBF changes of physiological significance. However, in any one brain the relative differences between integrated counts and estimated rCBF are so small, following global normalization, that parameter estimation is sometimes unnecessary. The justification for using integrated counts as a direct index holds given a strict condition; there is no *a priori* reason to expect a treatment effect on global measures. Treatment effects refer to those introduced by experimental design. It is unusual to find significant global differences in normal subjects during standard sensorimotor and cognitive activations. In our experience the only challenges that induce global differences are pharmacological. If the scope of the experimental question is limited to normal subjects, under physiological conditions, most investigators are comfortable using integrated counts per pixel as rCBF equivalents.

B. Stereotactic Differences

The coregister of homologous functional and anatomical loci from different subjects is the aim of stereotactic normalization. The simplifying assumption is that a correspondence exists between functional and structural anatomy. This assumption has been validated by the efficacy of stereotactic normalization in contributing to the detection of functional changes (Fox *et al.*, 1988). Stereotactic normalization is a data transformation that reduces differences in brain position, size, and shape by mapping the image data into a standard stereotactic space. The space most widely used is defined by the atlas of Talairach and Tournoux (1988) and was first proposed by Fox *et al.* (1985). This space has now become the international standard for communicating PET results.

There are two sorts of stereotactic variance, positional and morphological. Morphological differences have linear (size) and nonlinear (shape) components. Stereotactic normalization deals with these differences by reducing a single nonlinear three-dimensional problem to a series of one-dimensional linear problems.

1. Positional Variance

Positional variance is removed by translation and reorientation of the volume image with reference to a standard line, the intercommissural line passing through the anterior commissure (AC) and posterior commissure (PC). This is alternatively known as the AC–PC line. The position of the AC–PC line can be estimated directly from morphological information in the primary (PET) image without reference to a mediating structural (e.g., MRI) scan. This estimation uses the functional contrast at gray–white matter boundaries. The feasibility of doing this was first demonstrated by using four landmarks that could be identified on coronal PET sections and that bear a constant relationship to the AC–PC line (Friston *et al.*, 1989). The transverse level or height (z) of these landmarks was estimated for each of the coronal (y) levels. Linear regression was then used to estimate the AC–PC line. Construct validity was established with reference to the method described by Fox *et al.* (1985).

In order to increase reliability of the AC–PC line estimation the procedure has been automated; 15 coronal sections are sampled proportionally from the image. Each coronal section is matched, in a least-squares sense, to a standard template (average of many coronal sections following stereotactic normalization). This matching is in terms of z. The z displacement between the observed coronal section and the template defines the height of the AC–PC line. This procedure is repeated independently for all sections and the estimated AC–PC levels (z) regressed on the observed y. This regression is the AC–PC line estimate. Note that there is no explicit reference to the commissures or related structures. The functional profile over the entire brain volume contributes equally. In short, in contrast to earlier approaches, there are no morphometric landmarks because the procedure is correlative over the entire brain.

2. Brain Size

Brain size is defined by the bounding box in which it lies, the dimensions of which are simply determined by integrating the image over two dimensions to generate one-dimensional images. The lengths of these one-dimensional images are determined according to threshold criteria. Height is specified relative to the AC–PC line. The image is resliced parallel to the AC–PC line into 26 transverse sections that correspond to the drawings of the Talairach and Tournoux atlas (1988). These sections are linearly rescaled in x and y such that one pixel represents $2 \times 2 \times 4$ mm in the standard space.

3. Brain Shape

Each transverse section is mapped from Cartesian space to polar space. Each radius of the image in polar space is resampled according to the below theory: Let $g(x)$ be an observed continuous one-dimensional image (a radius of a polar image) and $\gamma(x)$ denote the desired image that approximates to a standard

template $\tau(x)$. The transformation $g(x) - \gamma(x)$ is effected by resampling $g(x)$ according to distortion of the space (x) described by $\phi(x)$:

$$\gamma(x) = g[\phi(x)] = \tau(x) + \sigma(x). \quad (1)$$

The difference between the observed image and the desired image is a slowly varying anatomical distortion in (of) space $[\phi(x)]$. The difference between the desired image and the template reflects a more rapidly varying difference due to functional changes $[\sigma(x)]$. All are continuous functions of x. The resampling function $\phi(x)$ is given by

$$\phi(x) \approx g^{-1}[\tau(x) + \sigma(x)], \quad (2)$$

assuming $g^{-1}(\cdot)$ and $\tau(\cdot)$ are smooth monotonic functions (see below),

$$\phi(x) \approx g^{-1}[\tau(x)] + g^{-1}[\sigma(x)] = g^{-1}[\tau(x)] + \varepsilon(x), \quad (3)$$

where $\varepsilon(x)$ is a high-frequency residual term. An estimate of $\phi(x)$ $[\phi'(x)]$ is obtained by applying the inverse image function to the template $g^{-1}[\tau(x)]$. The result is smoothed to reduce the effect of $\varepsilon(x)$ on the estimate $\phi'(x)$ [see Eq. (3)]. In practice, it is necessary to work with image integrals to ensure invertible, strictly increasing monotonic functions. For a fuller discussion, see Friston *et al.* (1991a). The key thing to note is that pixel values are not changed but moved according to the smooth resampling function. The smoothing affects the vectorial displacement of pixels $[\phi(x)]$, not the values themselves $[g(x)]$ (see Fig. 1).

This class of normalization has been validated by comparing linear and nonlinear sampling as described. In general cortical registration is significantly improved, whereas subcortical structures are less so. The approach is noniterative and noninteractive and therefore completely reliable.

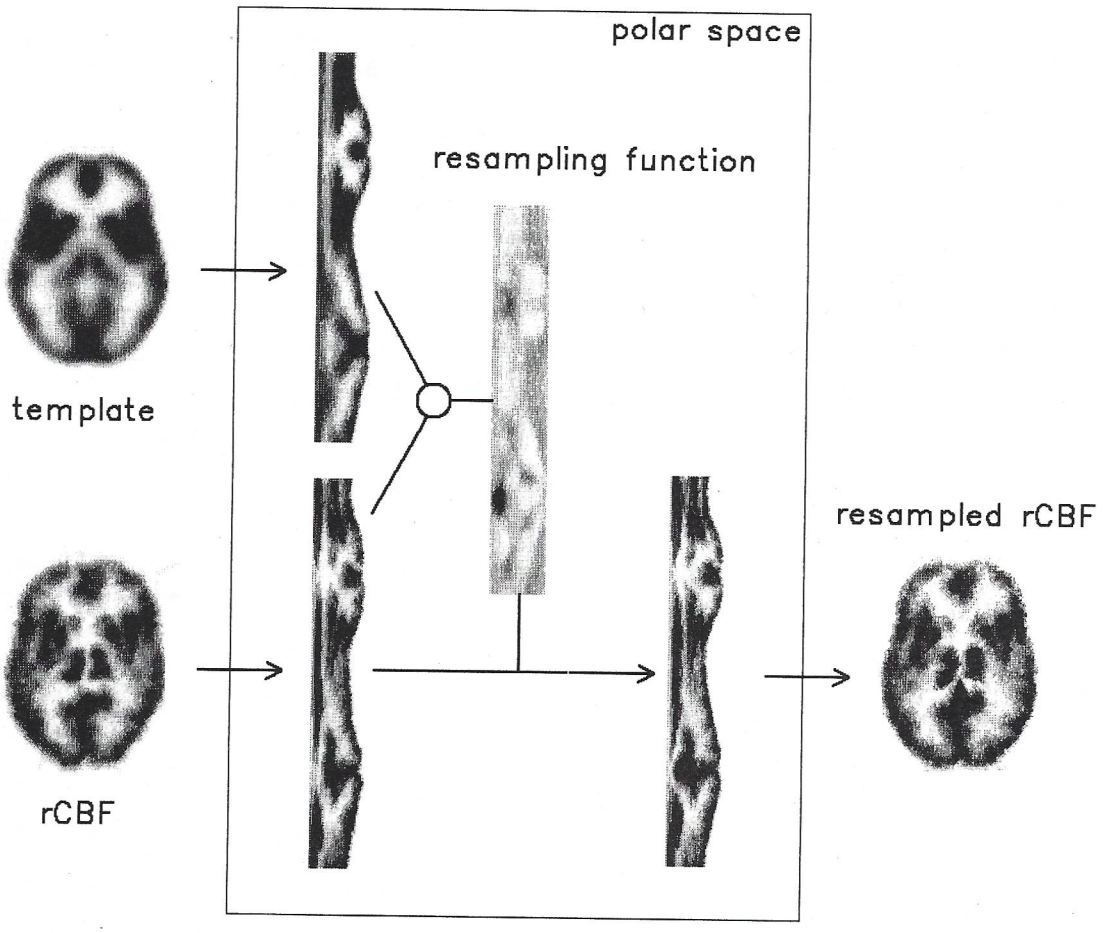

Figure 1 This schematic illustrates the nonlinear resampling of the Hoffman human brain phantom at 0 mm relative to the AC–PC line. Both observed $g(x)$ and template $\tau(x)$ sections are transformed from Cartesian to polar space and a resampling function $\phi(x)$ derived empirically for each radius (x) (row of the middle polar sections). The resampling function $\phi(x)$ is applied to the observed $g(x)$ polar section, which is then transformed back to Cartesian space. Brighter parts of the resampling function mean "resample the observed image from the left" (move to right) and darker parts mean "resample from the right." The derivation of $\phi(x)$ is described in the text.

C. Smoothing

1. Image Noise

This source of error variance can be reduced relative to signal by smoothing, or convolution. This is predicated on the observation that noise variance can be distributed in high spatial frequencies, whereas the signal cannot. The signal (differences in rCBF equivalents) must, by definition, have a spatial wavelength greater than the resolution of the acquisition system (because the signal must arise in resolvable structures). The highest spatial frequencies in noise are constrained only by the (Hanning) filter used in reconstruction (typically at 0.5 cycles per pixel).

2. Small-Scale Differences in Functional and Gyral Anatomy

There will always remain a spatial uncertainty about the position of a focal activation that remains after perfect stereotactic normalization. Functional specialization within a particular gyrus cannot be guaranteed from subject to subject and furthermore all subjects have slightly different gyral configurations. Convolution smooths a set of spatially dislocated activation foci into a center of common intersection. This intersection represents the cortical area evidencing a reliable increase in measured rCBF. Paradoxically the area of overlap can be smaller than the smoothing filter used, resulting in "hyperacute" spatial resolution.

Simulations and analytical solutions to maximizing this sort of signal recovery converge on surprisingly high degrees of smoothing. For typical resolutions of 8.5 mm (Spinks *et al.*, 1988), a Gaussian filter 20 mm in diameter is about optimal.

D. Global or Whole Brain Differences

A correction to rCBF estimates is usually required to account for the confounding effect of global CBF (gCBF) differences. This is achieved by covarying out the effect of gCBF using ANCOVA, a post hoc statistical adjustment with minimal assumptions. ANCOVA (Wildt and Ahtola, 1976; Friston *et al.*, 1990) is a generally accepted way of accounting for the effect of a nuisance variable or covariate (global activity for subject n under condition $k = G_{kn}$) on a dependent variable (observed rCBF = C_{kn}) to give an estimate of the subject independent, condition dependent variable (R_k) that would have been seen in the absence of covariate differences. The two linear models we have examined are defined by

$$C_{kn} = R_k + \beta(G_{kn} - E\{G_{kn}\}) \quad (4)$$

$$C_{kn} = R_k + \beta_k(G_{kn} - E\{G_{kn}\}), \quad (5)$$

where R_k is the adjusted regional index and $\beta_{[k]}$ is the regression slope (of C_{kn} on G_{kn}), reflecting the dependency of C_{kn} on G_{kn}. $E\{\cdot\}$ denotes expectation. Equation (4) contains only one term with a subscript k, and only k. This is the underlying regional effect that characterizes condition k. Because the regression slopes are parallel over all k conditions, the relative heights of the regression lines do not change with G_{kn}. For this reason, Eq. (4) is called the *independent model*. The activation effect from condition j to $i(R_i - R_j)$ does not depend on global activity. This can be remembered, somewhat metaphorically, by assuming that the physiological recruitment of cortical regions to perform a sensorimotor or cognitive operation does not depend on gCBF. Equation (5) is a more general case of Eq. (4) and allows for the regression slopes to change with condition $k(\beta_k)$. In this instance, the activation effect is two dimensional with an effect on R_k and an effect on β_k. Physiologically this is not easy to interpret. Because the activation component $(R_i - R_j)$ depends on the level of global activity (i.e., convergent or divergent regression lines), this equation is called the *dependent model*. Note a special case of Eq. (5) (when $\beta_k = R_k/E\{G_{kn}\}$),

$$C_{kn} = R_k + R_k(G_{kn} - E\{G_{kn}\})/E\{G_{kn}\}$$

i.e.,

$$R_k = C_{kn}/(G_{kn}/E\{G_{kn}\}), \quad (6)$$

is assumed in division by the whole brain mean. In this instance, the condition-specific, subject-independent factor (R_k) can be obtained by dividing the observed regional value (C_{kn}) by an estimate of the observed global index ($G_{kn}/E\{G_{kn}\}$). It is relatively straightforward to choose between Eqs. (4) and (5) by applying both to real data. Empirically it can be shown that applying the independent model [Eq. (4)] reveals a large number of pixels for which the null hypothesis that $R_i = R_j$ must be rejected. Conversely the dependent model [Eq. (5)] shows that the number of pixels for which β_k are different is less than chance expectation.

The rejection of the dependent model in favor of the independent model simplifies interpretation in that the activation effect is completely captured by an additive affect on R_k. See Fig. 2 for the regression analysis on real data implicit in the ANCOVA.

Marenco *et al.* (1991) find a substantial decrease in error variance and consequent increase in sensitivity with the ANCOVA model compared with division by global indices using SPECT and the Wisconsin Card Sort. Tempel *et al.* (1991) performed a regression anal-

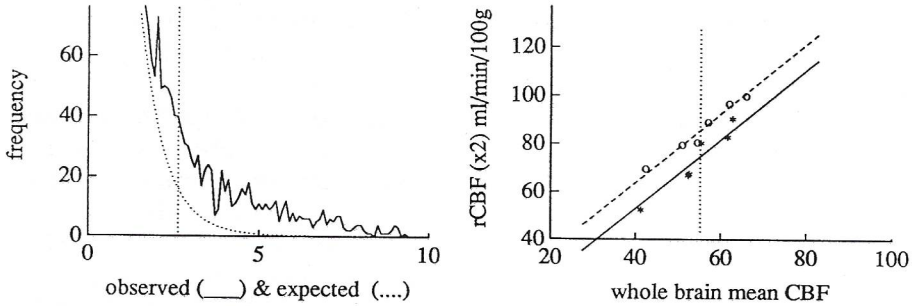

Figure 2 Right, the plotted regression analysis demonstrates graphically the effect of activation according to the *independent* ANCOVA model described in the text; namely, a vertical displacement in parallel regression lines of rCBF on gCBF. The solid line corresponds to a rest condition and the dotted line, a motor activation. Left, the distribution of the F ratio of variance attributable to treatment or condition and that due to error for all pixels in the slice from which the data in the regression were taken. Only the tail of the distribution is shown. The vertical line corresponds to $p < 0.05$. The solid line is the observed distribution and the dotted line, that expected under the null hypothesis.

ysis for several points during vibrotactile stimulation and rest and found only one example in which the B_k differed (at $p < 0.05$). Note that in the limiting case of $k = 1$ the ANCOVA adjustment reduces to a simple linear regression (see the study of schizophrenia below).

It is likely that the true relationship between relative regional and global indices is nonlinear, and therefore all linear models are invalid in a strict sense. The ANCOVA model with parallel regression slopes is probably the best, in that it allows for a linear approximation, over a small physiological range, to a generally nonlinear relationship.

E. Systematic Intersubject Differences

These are accounted for by using a completely randomized block design ANCOVA. The concept of a *block effect* accounts for the difference between a paired and an unpaired t test. The paired test is usually more sensitive because the variance not accounted for by the treatment is partitioned into true error variance and an intersubject (or block) variance. This refined modeling reduces the estimate of error variance and increases sensitivity. To generalize to k observations in n subjects, imagine an $n \times k$ data matrix with each subject along a row and conditions over columns. The means over columns and rows themselves have a variance. The variance of the means over rows represents error due to subject differences not under experimental control. This would normally contribute to error variance. It is this source of variance which is modeled and consequently removed by the block design. The variance in the k means over columns reflects diferences between the k conditions and has been introduced experimentally (treatment effect). Typically the block effect is about *twice* the treatment effect.

By convention the grand mean ($E\{G_{nk}\}$) is set to 50 (Mintun *et al.*, 1989; Fox *et al.*, 1989), such that rCBF means can be interpreted as estimates adjusted to a mean of 50 ml/min/dl. Note that these estimates are actually expressed in arbitrary units, which is particularly relevant if the original data were integrated counts per pixel. Unless rCBF is estimated formally using parameter estimation, they are referred to as rCBF equivalents.

F. Constructing the SPM

The adjusted rCBFs are subject to the appropriate statistical test and the results assembled pixel by pixel into the SPM. The nature of the SPM is as diverse as any statistic one can imagine, from a simple t test to the factor loading following a principal component analysis (see below). In what follows we concentrate on the general case of k conditions in n subjects.

The significance of a particular profile of changes in the (k adjusted condition mean) rCBFs is tested with a weighted sum of the mean rCBFs at each pixel. The weights used are called a *contrast* and are chosen to reflect the changes that one is interested in. For example in an $A\ B\ C\ C\ B\ A$ design, an activation in conditions A, with respect to conditions C, would be tested with the contrast $1\ 0\ -1\ -1\ 0\ 1$. If the observed rCBF means are highly correlated with the contrast, then the sum will be large. The weighted sum is divided by (a function of) the adjusted error variance, estimated at each pixel. The resulting quotient has the t distribution under the null hypothesis that there is no correlation between the time-dependent rCBF changes and the contrast specified. It is important

to note that the error variance used in constructing statistical parameteric maps is estimated for each brain region separately. This properly acknowledges that the underlying variablity in rCBF is not the same in different parts of the brain or under different experimental conditions. The use of contrasts preserves maximal flexibility by allowing pairwise, nonpairwise, orthogonal, nonorthogonal, and interaction comparisons. This flexibility takes comparison of condition means, and consequently experimental design, beyond a (cognitive) subtractive framework and into a more Boolean sphere. For example, conditions that are proposed to include a given cognitive component can be compared with all conditions that do not. This can be done even if no two brain states differ in, and only in, that component. Strictly speaking, a Boolean approach (e.g., what is in set A and is not in set B of conditions) should not become central, given that the contrast represents a linear sum of continuous variables.

This stage of analysis computes a t value for every pixel. Pixels at which the adjusted rCBF (equivalents) (mean over subjects and conditions) do not exceed 36 ml/min/dl are not analyzed further. Within the remaining (gray matter) brain regions a continuous smooth three-dimensional t image is created (SPM{t}). The object of further analysis is the interpretation of this direct test of the experimental hypothesis.

G. Assessing Significance

There are three approaches to interpreting the significance of SPMs (see Friston *et al.*, 1991b). Each is characterized by its own sort of null hypothesis (for computational and theoretical simplicity, the SPM{t} is actually transformed to the unit Gaussian distribution using a probability integral transform; this means changes are usually reported as Z scores).

1. Topographically Constrained Null Hypothesis

This is the simplest and states that there has been no change in rCBF at a single and specified brain location. This class of null hypothesis imposes a very selective interrogation of the data at, and only at, one brain region. Because of the smoothness inherent in the SPM{t} it is seldom necessary to specify the exact pixel *a priori*. This null hypothesis is rejected if the SPM{t} at the specified location exceeds, say, $p < 0.05$.

2. A Single Null Hypothesis Relating to the Profile of Activation

A profile of activation is defined as the *excursion set* of pixels above a threshold. There are as many activation profiles as thresholds. For any arbitrary threshold, the null hypothesis states that this profile could have occurred by chance. The chance expectation of any profile can be assessed with the probability of getting the observed number of pixels (x) in the excursion set, or more, by chance. To estimate this probability one needs to know the distribution of x under the null hypothesis. This approach to testing the overall significance of activation profiles was first proposed in Friston *et al.* (1990) using a Poisson approximation for the probability distribution of x. This form of omnibus testing has no localizing power but represents a nonarbitrary test for outliers. It is nonarbitrary because the pixels subtending the "improbability" of chance occurrence are explicitly identified by the threshold chosen.

While the Poisson approximation is asymptotically correct in the limit of no smoothness, it is probably not appropriate for SPMs with substantial smoothness. The problem here is that although the expectation of x is known exactly (it is determined by the known univariate distribution of the statistic in question, the threshold, and the total number of pixels analyzed) the variance of x depends on smoothing. Although smoothness increases the probability of getting a large number of pixels in the excursion set by chance it *decreases* the chance probability of getting a large number of contiguous sets of pixels (regions). This is used to advantage in the third approach to assessing significance, which introduces a correction for the number of pixels analyzed.

If no correction for multiple comparisons is made (see below) then the threshold is usually set at some reasonably high level (e.g., $p < 0.001$). A level of $p < 0.001$ has been shown to protect from false positives using phantom activation simulations (Bailey *et al.*, 1991). In some comparisons (for example where the block effect cannot be removed in comparing two different cohorts) a very low threshold is used (e.g. $p < 0.05$). At this level, given about $3 \cdot 10^4$ pixels are analyzed, the expectation under the null hypothesis is 1500 (a sphere of about 7 pixels radius).

3. Multiple Null Hypotheses for Each Pixel

The final approach to interpretation treats the SPM{t} as many nonindependent univariate tests. There are as many null hypotheses as there are pixels. If the null hypothesis of no change is rejected for a specific location, then an independent activation can be localized to this site irrespective of changes elsewhere. This requires a threshold correction for multiple comparisons or the large number of null hypotheses being tested concurrently. This correction is no

simple because the tests are not independent. Nonindependence is a consequence of smoothness.

For any given threshold the size of the excursion set will not depend on smoothness, but its spatial distribution will. A highly uncorrelated (rough) process will produce a large number of scattered regions subtending the excursion set. A very smooth process on the other hand is likely to have its entire excursion set in a single contiguous region. Although the univariate probability distribution of pixel values in the process is not a function of smoothness, the multivariate probability distribution of several neighboring pixels is. Account is taken of smoothing by defining the event of interest as the center of a contiguous subset of the excursion set (region). The probability (α) of this event (per pixel) is uniform over the image process and is a function of threshold (μ) and smoothness (s):

$$\alpha \approx (32 \cdot \pi \cdot s^2 \cdot \exp(\mu^2) \cdot p)^{-1}, \quad (7)$$

where p is equivalent probability in the absence of smoothing. s and FWHM are simply related:

$$\mathrm{FWHM} = 2.3548 \cdot s. \quad (8)$$

An appropriate correction for multiple nonindependent univariate comparisons requires $\alpha = 0.05/N$, where N is the total number of pixels analyzed and $\alpha \cdot N$ is the expected number of regions. The above approximation is used to determine the threshold. This determination requires an estimate of s, obtained from the variance of the SPM field derivatives. These results were developed using the theory of stochastic processes (Cox and Miller, 1987) [see Friston *et al.* (1991b) for a full exposition].

Recent work by Worsley *et al.* (1992) has used the Euler characteristic of the excursion set as an estimate of the number of contiguous suprathreshold regions. This related approach gives almost identical results (in two dimensions).

Any or all of the three different hypotheses described above could be applied to the same data. The distinction between exploratory and confirmatory studies is often reiterated. This distinction is repeatedly acknowledged by my colleagues with a benevolent, if weary, air. Clearly, imaging studies can be treated as both exploratory and confirmatory depending on the nature of the hypothesis being tested.

SPMs are usually displayed in their entirety by viewing the brain space from orthogonal directions and displaying the highest valued pixel along any line of view (maximum intensity projection). These orthogonal projections can be thought of as statistical X rays highlighting statistically dense (significant) regions. The data can be rendered onto drawings of the cortical surfaces to aid interpretation.

III. Applications

A. Functional Anatomy

1. An Activation Study

Consider this example from a six-subject study with three tasks presented twice (Frith *et al.*, 1991) ($n = 6$, $k = 6$). The tasks were presented in balanced order to avoid monotonic time effects (this is standard practice in some units)—*A B C C B A*, where *A* is a word shadowing task, *B* is a semantic opposites task, and *C* is a paced verbal fluency task. All tasks were paced at one word per 2 s. Words in tasks *A* and *B* were high-frequency, concrete words. The design of this paradigm was predicated on cognitive subtraction (Petersen *et al.*, 1989). The differences between *A* and *B* included semantic analysis, categorization, and retrieval. The key difference between *A* and *C* was the intentional aspect of word retrieval (intentional here means not specified by an extrinsic cue). This intensional component has been a major focus of our work using verbal fluency and memory challenges and reflects our interests in schizophrenia.

Figure 3 shows the comparison of tasks *C* and *A* (verbal fluency and word shadowing). The one-tailed SPM{t} were thresholded at $p = 0.001$ (no correction for multiple comparisons). The activation profile can be described as an extensive region in the left dorsolateral prefrontal cortex (DLPFC), including Broca's area (Brodmann's area, BA 44), and the anterior cingulate (bilaterally). There is a small region in the cerebellum that may or may not be significant. The decreases can be characterized as extensive bitemporal deactivations with a contribution from the posterior cingulate (bilateral). These are cursory but complete descriptions of the profiles. No one component of this profile is considered significant in its own right because a correction for multiple comparison was not made.

These results highlight a number of observations common to many cognitive activation profiles. First, if the cognitive differences between two tasks include an intentional component, the DLPFC is likely to be involved. Intentional tasks subsume (by definition) mnemonic tasks. Second, deactivations (rCBF decreases) characterize brain states with the same regional specificity and spatial extent typical of activations. Indeed one could look at the bitemporal deactivations as rCBF increases associated with extrinsically cued word generation (i.e., word shadowing

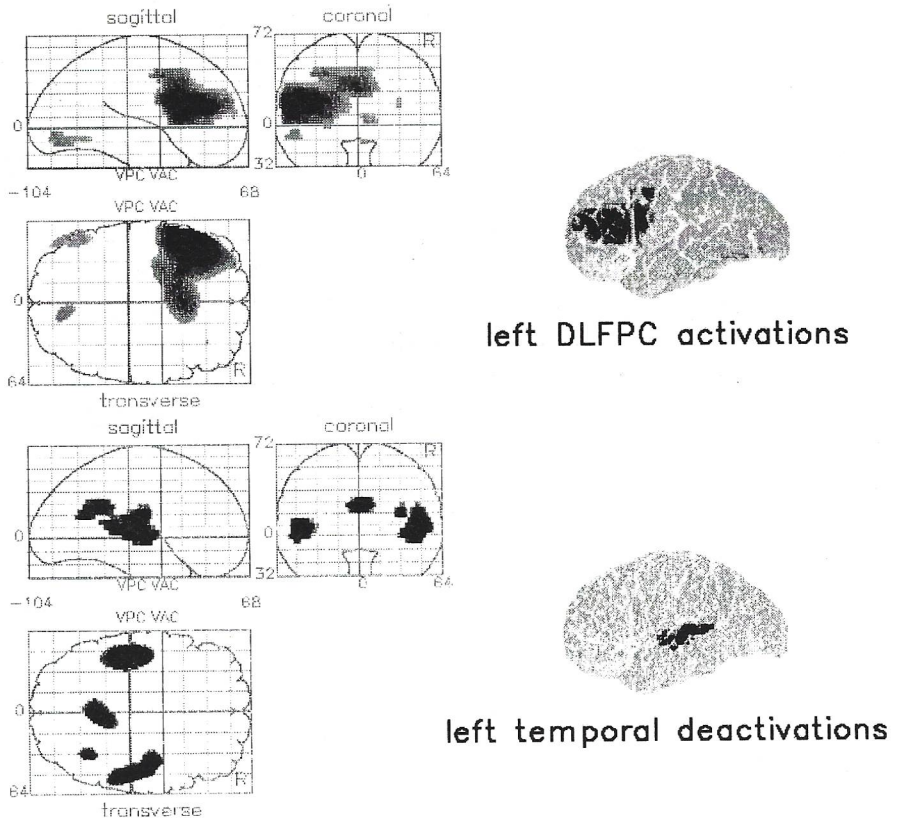

Figure 3 SPM{t} comparing two verbal fluency conditions with baseline (word shadowing conditions). The SPM has been thresholded at $p = 0.001$ with no correction for multiple comparisons. Because one-tailed levels were used, the increases (activations) and decreases (deactivations) are displayed separately. Each SPM{t} is displayed as a volume image from the back (top right), the side (top left), and top (bottom left) of the brain. The highest t value along any line of view is displayed. The standard stereotactic space is captured by the grid upon which the SPM{t} is superimposed (Talairach and Tournoux, 1988). The activation profile is described in the text but in summary shows a left DLPFC and bilateral anterior cingulate activation and bitemporal and posterior cingulate deactivations. The same excursion set of pixels has been divided into four sagittal blocks and the left lateral block, rendered onto a drawing of the cortical surface.

with verbal fluency as a control). Finally reciprocal changes in rCBF at remote sites is a common finding. Especially evident here are negatively correlated frontotemporal changes and a similar relationship between the anterior and the posterior parts of cingulate cortex. Both these correlations are seen in replication studies and other related (memory) paradigms.

2. Single Subjects and Single Conditions

The above is typical of the general $n \times k$ study. The SPM approach can be applied to many conditions in a single subject or indeed many subjects in the same state.

Figure 4 shows the rCBF increases attributed to morphine analgesia (see Jones *et al.*, 1991a). A 66-year-old man had had a well-differentiated squamous cell carcinoma of the left jaw, which was resected and irradiated. Four days after completion of radiotherapy, he could tolerate left-sided jaw pain without diamorphine analgesia. The subject was scanned nine times every 15 min. After three scans he received an intravenous morphine infusion at 10 mg/h. The first three scans (in pain) were compared with the last five (subjectively rated pain free). The corresponding SPM{t} thresholded at $p < 0.001$ (no correction for multiple comparisons) is seen in Fig. 4 and highlights substantial increases in the right DLPFC (contralateral to the site of pain) and anterior cingulate. The later finding is particularly interesting given the finding of anterior cingulate responses to pain in normal subjects (Jones *et al.*, 1991b; Talbot *et al.*, 1991).

Figure 5 shows left parahippocampal correlates of symptomatic severity in 30 chronic schizophrenics. Thirty DSMIII-R (American Psychiatric Association,

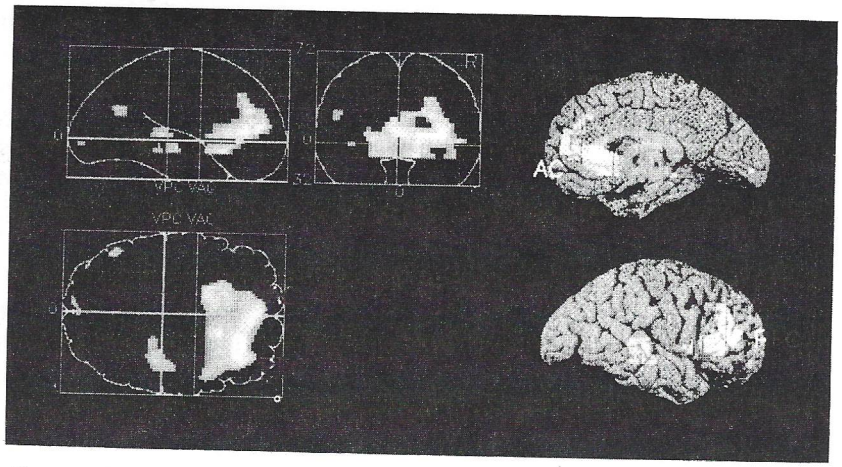

Figure 4 SPM{t} showing the significant increases ($p < 0.001$) in rCBF in a single subject repeatedly scanned during the induction of morphine analgesia.

1986) chronic schizophrenic patients all under the age of 55 were scanned under the same (rest) conditions. The selection criteria placed on emphasis on persistent and stable symptoms. Symptom ratings were made using CASH (Andreasen, 1987) and then subjected to factor analysis. This analysis revealed a three-dimensional structure to the behavioral data: psychomotor poverty, characterized by poverty of speech, movement, and feeling; a disorganization syndrome colored by inappropriate affect and incoherent speech with little informational content; and finally a dimension of positive experiential symptoms including delusions and hallucinations. The sum of these three factor scores provided an estimate of symptom severity that

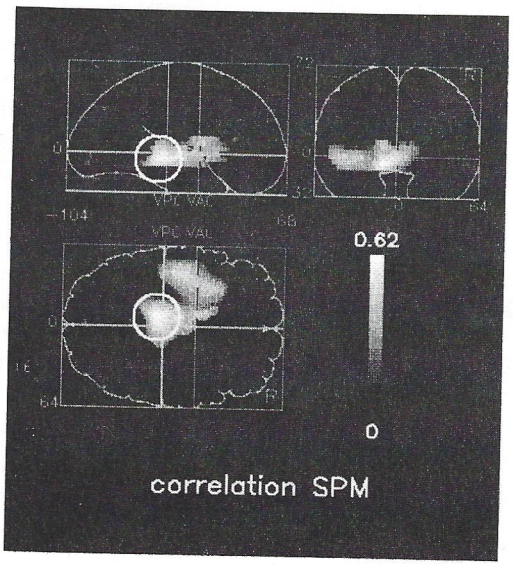

Figure 5 SPM{ρ} demonstrating marked positive correlations ($p < 0.05$) between symptom severity and adjusted rCBF in the left temporal region, mesencephalon, and basal ganglia (maximum correlation in the left parahippocampal gyrus-circled) in 30 DSMIII-R chronic schizophrenics.

received equal contributions from all (three) subsyndromes. This sum was correlated with adjusted rCBF at all pixels to generate a SPM{ρ}. Positive correlations thresholded at $p < 0.05$ (no correction for multiple comparisons) are displayed in Fig. 4. This statistic is equivalent to the partial correlation between overall symptom severity and rCBF, having accounted for the effect of global differences. The equivalent SPM{ρ} (not shown) for each of the separate subsyndromes revealed hypofrontality (Ingvar, 1974; DeLisi, 1985a, 1985b) for, and only for, the psychomotor poverty subsyndrome (see Liddle *et al.*, 1991; Friston *et al.*, 1992a).

Using the same analytical techniques and in particular the same standard stereotactic space allows the direct comparison of results on the functional anatomy of normal subjects and the physiological correlates of behavioral and cognitive deficits exhibited by patients. The relationship between stimulation experiments and disease or lesion studies has a long history in neuroscience. A landmark meeting, which took place on August 4th, 1881, to discuss localization of function in the cortex cerebri, addressed this issue. Goltz (1881), although accepting the results of electrical stimulation of the dog and monkey cortex (e.g., Ferrier, 1875), considered the excitation method inconclusive, in that movements elicited might have originated in related pathways or current could have spread to distant centers. "Ablation experiments were therefore essential to complement the results obtained by excitation" (Phillips *et al.*, 1984).

B. The Factorial Design—Cerebellar Plasticity

A natural extension of the SPM approach is the combination of two or more treatments in the same

activation study. The appeal of this (*factorial*) design is that both the main effects and the interaction between treatments are measurable. An interaction is simply a difference in differences, in other words, the modulation of activation attributable to one treatment by a second. The first PET experiment in this class was perhaps the simplest imaginable and will serve as a concrete illustration of the idea.

Consider the synaptic changes that underlie motor learning. The cerebellum has long been thought to be implicated in motor learning (Marr, 1968; Albus, 1971; Ito *et al.*, 1974). Gilbert and Thach (1977) have demonstrated a reduction in the simple and complex spike activity of Purkinje cells in the cerebellum during motor learning in nonhuman primates. At a synaptic level, long-term depression (LTD) at synapses on apical dendrites of Purkinje cells, at the site of contact with parallel fibers, in neocerebellar cortex may be a key mechanism. Ito and colleagues (1989) have demonstrated LTD in synaptic efficacy following conjoint stimulation of parallel fibers and climbing fibers. If LTD in the neocerebellar cortex is associated with repeated practice of a novel motor task, it should be possible to image the neurophysiological correlates of these changes. It might be expected that physiological adaptation of the response to motor performance would be seen in the neocerebellum and the target area of Purkinje cell afferents (cerebellar nuclei) one synapse downstream. To test this hypothesis, subjects repeated *rest-finger opposition* task pairs three times. To ensure performance changes did not confound interpretation, finger opposition was entrained with a metronome. The two treatments in this example were *motor activation* and *time*. Motor activation had two levels (rest and practice) and time had three (first, second, and third trial pairs). The interaction term corresponds to physiological adaptation of the motor activation, namely an attenuation of the motor activation effect on rCBF over time (a difference in the differences). The results of this study (Friston *et al.*, 1992b, 1991c) were consistent with LTD in the cerebellum. Figure 6 shows two SPM{*t*}. The first represents the main effect of motor performance and is a typical motor activation profile (Deiber *et al.*, 1990). The second SPM{*t*} is the interaction term. This profile is strongest in the cerebellar cortex (ipsilateral to hand moved) and cerebellar nuclei. Additional components include the brain stem at the level of the inferior colliculi and a small portion of SMA (no data were obtained above this level). The contrasts (or weights) used to create the SPM{*t*} were:

	Condition (R, rest; A, practice)					
	R	A	R	A	R	A
Main effect of motor activation	−1	1	−1	1	−1	1
Interaction	−1	1	0	0	1	−1

There were no main effects of time at the threshold used ($p < 0.001$).

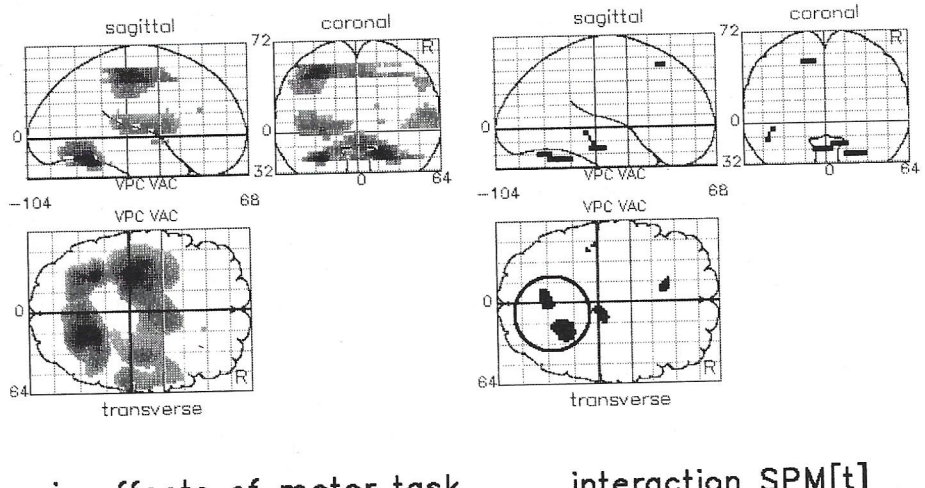

Figure 6 SPM{*t*}s depicting the main effect of motor activation and the interaction effect between motor activation and time (trial number). The one-tailed SPM{*t*}s are thresholded at $p = 0.001$ with no correction for multiple comparisons. The left SPM{*t*} shows increases and highlights the motor system from sensorimotor cortex to ipsilateral cerebellum. The interaction SPM{*t*} reflects adaptation of the activation effect. The components subtending this profile include the ipsilateral neocerebellum, the cerebellar midline at the level of the cerebellar nuclei, the brain stem, and a small portion of SMA at the edge of the field of view of the camera.

One clear application of the factorial design is to cross psychological and pharmacological treatments in a combined psychopharmacological paradigm. Indeed the study of neuromodulatory neurotransmitter systems requires a second treatment to elicit a physiological response that can be modulated (neuromodulation is here defined as an induced change in physiological response to an independent afferent input). This approach has been used with particular success by crossing subsupraspan memory tasks with the $5HT_{1A}$ partial agonist buspirone and the mixed dopamine agonist apomorphine (see Friston *et al.*, 1992c; Grasby *et al.*, 1992).

C. Functional and Effective Connectivity

In the past two decades the concept of *functional* or *effective connectivity* has been most thoroughly elaborated in the analysis of multiunit recordings of separable neuronal spike trains, recorded simultaneously from different brain areas (Gerstein and Perkel, 1969; Gerstein *et al.*, 1989). Temporal coherence among the activity of different neurones is commonly measured by cross-correlating their spike trains. The resulting correlograms are then interpreted as the signature of effective connectivity. In current approaches, effective connectivity is assessed as the joint probability of two neurones firing together as a function of time in an interstimulus interval (Aertsen and Preissl, 1991). There is a close relationship between the notion of effective connectivity and synaptic *efficacy*; "It is useful to describe the effective connectivity with a connectivity matrix of effective synaptic weights. Matrix elements would represent the effective influence by neurone i on neurone j" (Gerstein *et al.*, 1989). This definition is an essential and useful abstraction but lacks operational significance. In what follows, we reserve the term functional connectivity to mean *the observed temporal correlation between two electro/neurophysiological measurements from different parts of the brain*. Effective connectivity will refer to the underlying efficacy, which may or may not be measurable.

An exposition of functional connectivity based on PET physiological data can be reduced to an examination of its correlation structure. Correlation structure refers to the correlations observed over a time series in the same subject(s) (e.g., Friston *et al.*, 1991d; Lagreze *et al.*, 1991). This is very different from the analysis of correlations in cross-sectional data (acquired in different subjects in a single state). See Metter *et al.* (1984), Moeller *et al.* (1987), and Horwitz *et al.* (1984, 1990, 1991) for notable contributions to this related but separate field. Principal component analysis (PCA), as a first step, is most suited to the examination of correlations in a time series (Hope, 1968). PCA extracts the important features of the correlation matrix in terms of principal components or eigenvectors. This approach is formally equivalent to the derivation of orthonormal spatial nodes from multiunit electrode recordings or multichannel EEGs [see the many chapters in Dvorak and Holden (1991)]. Spatial modes represent an elegant reorganization of a time series into a small number of distributed patterns. Within each mode, there are high correlations or high functional connectivity. Conversely, the temporal dynamics of different spatial modes are independent. Temporal dynamics refer to how much each mode contributes to activity over time.

The PCA of imaging data is not straightforward in the sense that the volume of data can be vast. This leads to computational memory problems when trying to find the principal components associated with the data covariance matrix. The simplest way to identify the principal components (eigenimages) is to use Singular Value Decomposition where:

$$[U\lambda V] = \mathrm{SVD}\{M^{\mathrm{T}}\}$$

and

$$M^{\mathrm{T}} = U.\lambda V^{\mathrm{T}}. \tag{9}$$

M is the data matrix with one column per pixel. U and V are unit matrices and λ is a diagonal matrix of singular values. Assuming M has been normalized to zero mean over columns, the eigenvector solution of the covariance matrix of $M(C\{M\})$ is simply U:

$$C\{M\} = M^{\mathrm{T}}.M = U.\lambda^2.U^{\mathrm{T}}$$

or

$$C\{M\}.U = U.\lambda^2. \tag{10}$$

An alternative approach was presented in Friston *et al.* (1993), which uses a recursive self calling algorithm. The advantage of recursive PCA over SVD is (a) that the entire data matrix does not have to be in working memory at any time and (b) recursive PCA lends itself to implementation on a parallel architecture. The disadvantages of recursive PCA are (a) it is more computationally expensive (requires more floating point operations) and (b) requires M to have a power of 2 columns.

1. Recursive PCA Analysis

The technique is modeled on "L" systems or string rewriting systems used in the construction of fractal and self-similar patterns. L systems were introduced by Lindenmayer in 1968 to model the growth of living organisms. In these systems, a pattern (primitive) that is composed of line segments is defined. According to (production) rules, each segment is replaced by the scaled pattern primitive. This primitive is constructed

from line segments that are recursively replaced with smaller scaled primitives. No "drawing" actually occurs until the scale reaches a specified lower limit. See Voss (1988) for a full discussion. The charm of these systems is that the algorithm, which replaces each line segment of the primitive with smaller versions, calls itself recursively but implements pattern drawing only at the smallest scale. In a similar way, the PCA used here recursively calls itself until the size of the primitive data matrix reaches a lower limit. Let $\theta(M)$ denote the operation of the PCA operator $\theta\{\cdot\}$ on a data matrix (M), where M can be bisected $[M = (M_1 M_2)]$. The algorithm is defined by the following equivalence,

$$\theta\{M\} = \begin{pmatrix} \theta\{M_1\} & 0 \\ 0 & \theta\{M_2\} \end{pmatrix} \cdot \theta\{(M_1 \cdot \theta\{M_1\} M_2 \cdot \theta\{M_2\})\}, \tag{11}$$

until the size of M reaches a lower limit ($S \geq 2.\text{rank}(M)$). Then

$$\theta\{M\} = \varepsilon\{C\{M\}\} = Q_k, \tag{12}$$

where Q_k are the largest $S/2$ eigenvectors of the covariance matrix of M $(= C\{M\})$. The operator $\theta\{\cdot\}$ recursively calls itself until the multiply bisected subpartitions reach a stopping criterion in terms of size (S) [see Friston *et al.* (1993) for a full description]. It should be noted that the key proposal here is that principal components or eigenimages are a powerful reorganization of the data and are directly related to the concept of functional connectivity. SVD and recursive PCA represent two computationally efficient ways of obtaining these eigenimages.

To pursue the functional connectivity implicated by intentional behavior, we repeated the word generation paradigm described above using word shadow-

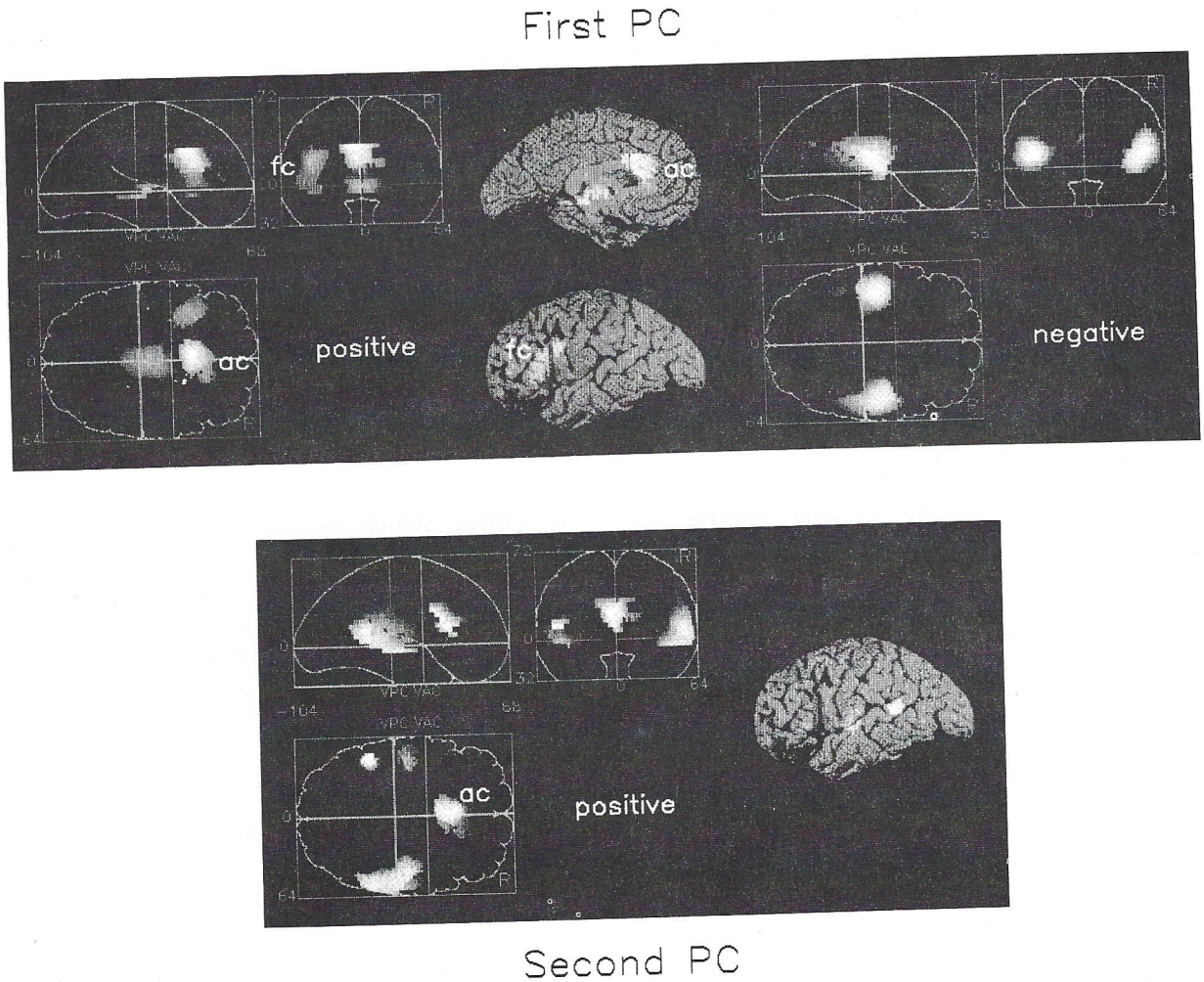

Figure 7 SPM{PC_1^+}, SPM{PC_1^-}, and SPM{PC_2^-}. First and second spatial modes for all voxels entered into the analysis (those with a nontrivial $F: p < 0.05$ following ANCOVA). Positive and negative loadings are shown for the first PC. Only positive loading are displayed for the second PC. ac, anterior cingulate; fc, left prefrontal cortex.

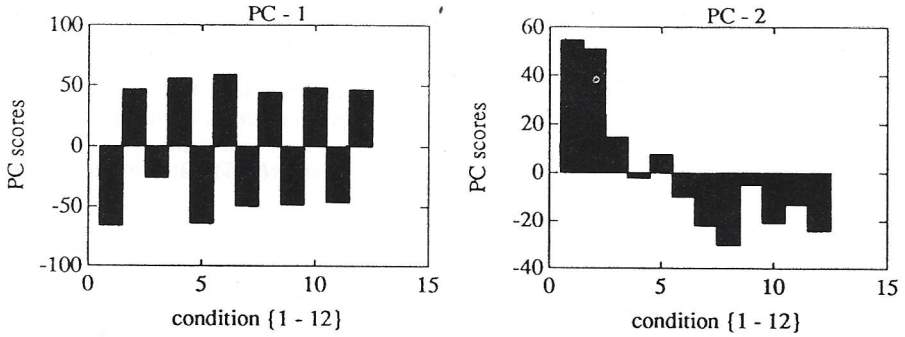

Figure 8 PC scores for the first two PCs or spatial modes. Conditions are baseline, fluency, baseline, ... These patterns suggest the first spatial mode is engaged by the task (i.e., variance introduced by experimental design). The second mode appears to reflect adaptation of absolute rCBF over the entire experiment.

ing and verbal fluency. Six subjects performed the two tasks alternately for 12 scans (order balanced across subjects). The mean adjusted rCBF equivalents for each of the $k = 12$ conditions were subject to recursive PCA analysis. The first two principal components, or spatial modes, accounted for almost all the variance observed (86%). The first mode accounted for 71% and the second, for 15% of variance. These are seen in Fig. 7. The third mode accounted for only 4%. The first spatial mode had positive loadings in the anterior cingulate (Brodmann's area, BA 24,32), the left dorsolateral prefrontal cortex (DLPFC BA 46) and Broca's area (BA 44), the thalamic nuclei, and the cerebellum. Negative loadings were seen bitemporally and in the posterior cingulate. This profile is a verbal fluency profile we discussed above (Fig. 3) (Frith *et al.*, 1991). We have not observed subcortical activation to be so reliable in previous data. The PC scores, reflecting the contribution of spatial modes to each condition (Fig. 8), testify to this interpretation. The first mode is very evident in the verbal fluency tasks, with correspondingly low scores on the baseline. Furthermore, these scores are largely invariant over time. The second principal component had its highest positive loading in the anterior cingulate and appears to correspond to a monotonic time effect with greatest prominence in the first three conditions (Fig. 8).

The two spatial modes may represent an *intentional* system critical for the intrinsic generation of words and a second *attentional* system whose physiology changes monotonically with time. This adaptation could reflect a decline in acquisition of perceptual set (Wise, 1989) as the tasks become familiar [see Posner *et al.* (1990) and Pardo *et al.* (1990) for evidence implicating the anterior cingulate in attention].

The functionally connected system corresponding to the first principal component accounted for 71% of the observable differences in adjusted mean rCBF from the 12 scans. This is a remarkable observation in that 71% of the variance in brain physiology was introduced by experimental design. This is a clear vindication of the PET technique in the investigation of functional anatomy and connectivity. Furthermore, the distributed system highlighted is in exact accord with that predicted from anatomical connectivity. All the components of this system (anterior cingulate, DLPFC, posterior cingulate, and superior temporal region) have dense and reciprocal connections (Pandta and Barnes, 1987; Goldman-Rakic, 1987, 1988).

IV. Conclusion

As the last section leaves us in a recursive frame of mind, the reader is referred to the introduction.

Acknowledgments

Thanks to colleagues at the MRC Cyclotron Unit for their contributions at both intellectual and technical levels. K.J.F. was funded by the Wellcome Trust during this work.

References

Aertsen, A., and Preissl, H. (1991). Dynamics of activity and connectivity in physiological neuronal networks. *In* "Non Linear Dynamics and Neuronal Networks" (Ed Schuster, Ed.), pp. 281–302. New York: HG VCH Publishers.

Albus, J. S. (1971). A theory of cerebellar function. *Math. Biosci.* **10,** 25–61.

American Psychiatric Association (1987). "Diagnostic and Statistical Manual of Mental Disorders," third ed. Washington, D.C.: American Psychiatric Press.

Andreasen, N. C. (1986). "Comprehensive Assessment of Symptoms and History." Iowa City, Iowa: University of Iowa, College of Medicine.

Bailey, D. L., Jones, T., Friston, K. J., Colebatch, J. G., and Frackowiak, R. S. J. (1991). Physical validation of statistical parameteric mapping. *J. Cereb. Blood Flow Metab.* **11**(Suppl. 2), S150.

Collings, S. N. (1977). "Mathematical Statistics: Its Setting and Scope," pp. 73–75. Milton Keynes, United Kingdom: The Open University Press.

Cox, D. R., and Miller, H. D. (1980). "The Theory of Stochastic Processes," pp. 272–336. New York: Chapman & Hall.

Deiber, N. P., Passingham, R. E., Colebatch, J. G., Friston, K. J., Nixon, P. D., and Frackowiak, R. S. J. (1991). Cortical areas and the selection of movement. *Exp. Brain Res.* **84,** 393–402.

Delisi, L. E., Holcomb, H., Cohen, R. M., *et al.* (1985a). Positron emission tomography in patients with and without neuroleptic medication. *J. Cereb. Blood Flow Metab.* **5,** 201–206.

Delisi, L. E., Buchsbaum, M. S., Holcomb, H., *et al.*, (1985b). Clinical correlates of decreased anteroposterior metabolic gradients in positron emission tomography (PET) of schizophrenic patients. *Am. J. Psych.* **142,** 78–81.

Dvorak, I., and Holden, A. V. (Eds.) (1991). "Mathematical Approaches to Brain Functioning Diagnostics," pp. 1–463. New York: Manchester University Press.

Ferrier, D. (1875). Experiments on the brain of monkeys. *Proc. R. Soc. London* **23,** 409–430.

Fox, P. T., Perlmutter, J. S., and Raichle, M. E. (1985). A stereotactic method of anatomical localization for positron emission tomography. *J. Comput. Assist. Tomogr.* **9,** 141–153.

Fox, P. T., Mintun, M. A., Reiman, E. M., and Raichle, M. E. (1988). Enhanced detection of focal brain responses using intersubject averaging and change distribution analysis of subtracted PET images. *J. Cereb. Blood Flow Metab.* **8,** 642–653.

Fox, P. T., and Mintun, M. A. (1989). Non-invasive functional brain mapping by change distribution analysis of averaged PET images of $H^{15}O_2$ tissue activity. *J. Nucl. Med.* **30,** 141–149.

Friston, K. J., Passingham, R. E., Nutt, J. G., Heather, J. D., Sawle, G. V., and Frackowiak, R. S. J. (1989). Localization in PET images: Direct fitting of the intercommissural (AC–PC) line. *J. Cereb. Blood Flow Metab.* **9,** 690–695.

Friston, K. J., Frith, C. D., Liddle, P. F., Lammertsma, A. A., Dolan, R. J., and Frackowiak, R. S. J. (1990). The relationship between local and global changes in PET scans. *J. Cereb. Blood Flow Metab.* **10,** 458–466.

Friston, K. J., Frith, C. D., Liddle, P. F., and Frackowiak, R. S. J. (1991a). Plastic transformation of PET images. *J. Comput. Assist. Tomogr.* **15,** 634–639.

Friston, K. J., Frith, C. D., Liddle, P. F., and Frackowiak, R. S. J. (1991b). Comparing functional (PET) images: The assessment of significant change. *J. Cereb. Blood Flow Metab.* **11,** 690–699.

Friston, K. J., Frith, C. D., Liddle, P. F., and Frackowiak, R. S. J. (1991c). The cerebellum in skill learning. *J. Cereb. Blood Flow Metab.* **11**(Suppl. 2), S440.

Friston, K. J., Frith, C. D., Liddle, P. F., and Frackowiak, R. S. J. (1991d). Investigating a network model of word generation with positron emission tomography. *Proc. R. Soc. London B* **244,** 101–106.

Friston, K. J., Liddle, P. F., Frith, C. D., Hirsch, S. R., and Frackowiak, R. S. J. (1992a). The left medial temporal lobe and schizophrenia: A PET study. *Brain* **115,** 367–382.

Friston, K. J., Frith, C. D., Liddle, P. F., and Frackowiak, R. S. J. (1992b). Motor practice and neurophysiological adaptation in the cerebellum: A positron emission study. *Proc. R. Soc. London B* **248,** 223–228.

Friston, K. J., Grasby, P., Bench, C., Frith, C. D., Cowen, P. J., Liddle, P. F., and Frackowiak, R. S. J. (1992c). Measuring the neuromodulatory effects of drugs in man with positron tomography. *Neurosci. Lett.* **141,** 106–110.

Friston, K. J., Frith, C. D., Liddle, P. F., and Frackowiak, R. S. J. (1993). Functional connectivity: The principal component analysis of large (PET) data sets. *J. Cereb. Blood Flow Metab.* **13,** 5–14.

Frith, C. D., Friston, K. J., Liddle, P. F., and Frackowiak, R. S. J. (1991). Willed action and the prefrontal cortex in man. *Proc. R. Soc. London B* **244,** 241–246.

Gerstein, G. L., and Perkel, D. H. (1969). Simultaneously recorded trains of action potentials: Analysis and functional interpretation. *Science* **164,** 828–830.

Gerstein, G. L., Bedenbaugh, P., and Aertsen, A. M. H. J. (1989). Neuronal assemblies. *IEEE Trans. Biomed. Eng.* **36,** 4–14.

Gilbert, P. F. C., and Thach, W. T. (1977). Purkinje cell activity during motor learning. *Brain Res.* **128,** 309–328.

Goldman-Rakic, P. S. (1987). Circuitry of primate frontal cortex and the regulation of behavior by representational memory. *In* "Handbook of Physiology: The Nervous System" (F. Plum and V. Mountcastle, Eds.), Vol. 5, pp. 373–417. Baltimore: Williams & Wilkins.

Goldman-Rakic, P. S. (1988). Topography of cognition: Parallel distributed networks in primate association cortex. *Annu. Rev. Neurosci.* **11,** 137–156.

Goltz, F. (1881). *In* "Transactions of the Seventh International Medical Congress" (W. J. W. MacCormac, Ed.), Vol. 1, pp. 218–228. London: Kolkmann.

Grasby, P. M., Friston, K. J., Bench, C., Cowen, P. J., Frith, C. D., Liddle, P. F., Frackowiak, R. S. J., and Dolan, R. J. (1992). The effects of the 5HT1A partial aginist buspirone on regional cerebral blood flow in man. *Psychopharmacology* **108,** 380–386.

Hope, K. (1968). "Methods of Multivariate Analysis," p. 64. London: University of London Press.

Horwitz, B., Duara, R., and Rappoport, S. I. (1984). Intercorrelations of glucose rates between brain regions: Application to healthy males in a reduced state of sensory input. *J. Cereb. Blood Flow Metab.* **4,** 484–499.

Horwitz, B. (1990). Simulating functional interactions in the brain: A model for examining correlations between regional cerebral metabolic rates. *Int. J. Biomed. Comput.* **26,** 149–170.

Horwitz, B., Grady, C., Haxby, J., Schapiro, M., Carson, R., Herscovitch, P., Ungerleider, L., Mishkin, M., and Rapoport, S. (1991). Object and spatial visual processing: Intercorrelations of regional cerebral blood flow among posterior brain regions. *J. Cereb. Blood Flow Metab.* **11,**(Suppl. 2), S380.

Ingvar, D. H., and Franzen, G. (1974). Abnormalities of cerebral blood flow distribution in patients with chronic schizophrenia. *Acta Psych. Scand.* **50,** 425–436.

Ito, M., Shida, T., Yagi, N., and Yamamoto, M. (1974). The cerebellar modification of rabbit's horizontal vestibulo-ocular reflex induced by sustained head rotation combined with visual stimulation. *Proc. Jpn. Acad. Sci.* **50,** 85–89.

Ito, M. (1989). Long term depression. *Annu. Rev. Neurosci.* **12,** 85–102.

Jones, A. K. P., Brown, W. D., Friston, K. J., Qi, L. Y., and Frackowiak, R. S. J. (1991a). Cortical and subcortical responses to pain in man using positron emission tomography. *Proc. R. Soc. London B* **244,** 39–44.

Jones, A. K. P., Friston, K. J., Qi, L. Y., Harris, M. Cunningham, V. J., Jones, T., Feinman, C., and Frackowiak, R. S. J. (1991b). Sites of action of morphine in the brain. *Lancet,* 338–825.

Liddle, P. F., Friston, K. J., Frith, C. D., Jones, T., Hirsch, S. R.,

and Frackowiak, R. S. J. (1992). Patterns of cerebral blood flow in schizophrenia. *Br. J. Psych.* **160,** 179–186.

Lagreze, H. L., Hartmann, A., and Shaub, L. (1991). A factor imaging of cortical blood flow during behavior activation: Interaction of neuronal networks in cognition. *J. Cereb. Blood Flow Metab.* **11,** S369.

Lammertsma, A. A., Cunningham, V. J., Deiber, M. P., Heather, J. D., Bloomfield, P. M., Nutt, J. G., Frackowiak, R. S. J., and Jones, T. (1990). Combination of dynamic and integral methods for generating reproducible functional CBF images. *J. Cereb. Blood Flow Metab.* **10,** 675–686.

Marenco, S., Coppola, R., Daniel, D. G., Zigun, J. R., Gorey, J. G., Jones, D. W., Berman, K. F., and Wienberger, D. R. (1991). rCBF activation with the Wisconsin card sort test in normal and schizophrenic subjects measured by SPECT. *J. Cereb. Blood Flow Metab.* **11**(Suppl. 2), S822.

Marr, D. (1969). A theory of cerebellar cortex. *J. Physiol.* **202,** 437–470.

Metter, E. J., Riege, W. H., Kuhl, D. E., and Phelps, M. E. (1984). Cerebral metabolic relationships for selected brain regions in healthy adults. *J. Cereb. Blood Flow Metab.* **4,** 1–7.

Mintun, M. A., Fox, P. T., and Raichle, M. E. (1989). A highly accurate method of localizing regions of neuronal activation in the human brain with positron emission tomography. *J. Cereb. Blood Flow Metab.* **9,** 96–103.

Moeller, J. R., Struther, S. C., Sidtis, J. J., and Rottenberg, D. A. (1987). Scaled subprofile model: A statistical approach to the analysis of functional patterns in positron emission tomographic data. *J. Cereb. Blood Flow Metab.* **7,** 649–658.

Pandya, D. N., and Barnes, C. L. (1987). Architecture and connections of the frontal lobes. *In* "The Frontal Lobes Revisited," pp. 41–71. The IRBN Press.

Pardo, J. V., Pardo, P. J., Janer, K. W., and Raichle, M. E. (1990). The anterior cingular cortex mediates processing selection in the Stroop attentional conflict paradigm. *Proc. Natl. Acad. Sci. USA* **87,** 256–259.

Petersen, S. E., Fox, P. T., Posner, M. I., Mintun, M., and Raichle, M. E. (1989). Positron emission tomographic studies of the processing of single words. *J. Cog. Neurosci.* **1,** 153–170.

Phillips, C. G., Zeki, S., and Barlow, H. B. (1984). Localization of function in the cerebral cortex: Past present and future. *Brain* **107,** 327–361.

Posner, M. L., Sandson, J., Dhawan, M., and Shulman, G. L. (1990). Is word recognition automatic? A cognitive–anatomical approach. *J. Cog. Neurosci.* **1,** 50–60.

Spinks, T. J., Jones, T., Gilardi, M. C., and Heather, J. D. (1988). Physical performance of the latest generation of commercial positron scanner. *IEEE Trans. Nucl. Sci.* **35,** 721–725.

Talairach, J., and Tournoux, P. (1988). "A Coplanar Stereotaxic Atlas of a Human Brain." Stuttgart: Thieme.

Talbot, J. D., Marrett, S., Evans, A. C., Meyer, E., Boshnell, and M. C., Duncan, G. H. (1991). Multiple representations of pain in human cerebral cortex. *Science* **251,** 1355–1358.

Tempel, L. W., Snyder, A. Z., and Raichle, M. E. (1991). PET measurement of regional and global cerebral blood flow at rest and with physiological activation. *J. Cereb. Blood Flow Metab.* **11**(Suppl. 2), S367.

Voss, R. F. (1988). Fractals in nature: From characterization to stimulation. *In* "The Science of Fractal Images" (H. Peitgen and D. Saupe, Eds.), pp. 21–69. New York: Springer-Verlag.

Wildt, A. R., and Ahtola, O. T. (1978). "Analysis of Covariance," p. 30. Beverly Hills/London: Sage Publications.

Wise, S. P. (1989). Frontal cortical activity and motor set. *In* "Neural Programming" (M. Ito, Ed.), p. 26. Tokyo: Japanese Scientific Societies Press.

Worsley, K. J., Evans, A. C., Marrett, S., and Neelin, P. (1992). A three-dimensional statistical analysis for rCBF activation studies in human brain. *J. Cereb. Blood Flow Metab.* **12,** 900–918.